

OPEN ACCESS

EDITED BY
Jasper Iske,
Brigham and Women's Hospital, Harvard
Medical School, United States

REVIEWED BY Antu Das, University of Pittsburgh, United States Yiming Zhao, First Affiliated Hospital of Xi'an Jiaotong University, China

*CORRESPONDENCE
Jie Zhao

☑ zjsecond@aliyun.com

[†]These authors have contributed equally to this work and share first authorship

RECEIVED 10 June 2025 ACCEPTED 19 August 2025 PUBLISHED 23 September 2025

CITATION

Zhang X, Zhang W, Wei J, Jin S, Wang Z, Wang H, Feng G and Zhao J (2025) GlyT1 inhibition by ALX-5407 attenuates allograft rejection through suppression of Th1 cell differentiation. *Front. Immunol.* 16:1644529. doi: 10.3389/fimmu.2025.1644529

COPYRIGHT

© 2025 Zhang, Zhang, Wei, Jin, Wang, Wang, Feng and Zhao. This is an open-access article distributed under the terms of the Creative Commons Attribution License (CC BY). The use, distribution or reproduction in other forums is permitted, provided the original author(s) and the copyright owner(s) are credited and that the original publication in this journal is cited, in accordance with accepted academic practice. No use, distribution or reproduction is permitted which does not comply with these terms.

GlyT1 inhibition by ALX-5407 attenuates allograft rejection through suppression of Th1 cell differentiation

Xiaohan Zhang^{1,2†}, Weiqi Zhang^{1,2†}, Jianghao Wei², Shuai Jin^{2,3}, Zhen Wang², Hui Wang², Gang Feng² and Jie Zhao^{2*}

¹Research Institute of Transplant Medicine, School of Medicine, Tianjin First Central Hospital, Nankai University, Tianjin, China, ²Department of Renal Transplantation, Tianjin First Central Hospital, Nankai University, Tianjin, China, ³The First Central Clinical School, Tianjin Medical University, Tianjin, China

Objective: Transplant rejection driven by Th1 cell-mediated immune responses remains a critical challenge. This study aimed to investigate the role of glycine transporter 1 (GlyT1/SLC6A9) in Th1 differentiation and evaluate the therapeutic potential of its inhibitor, ALX-5407, in attenuating allograft rejection.

Methods: RNA sequencing, flow cytometry, and qRT-PCR were employed to analyze GlyT1 expression in Th1-polarized CD4⁺T cells. ALX-5407 (0.5–500 nM) was tested *in vitro* under Th1-polarizing conditions. A murine skin allograft model (BALB/c to C57BL/6) was established to assess graft survival and immune responses. Combination therapy with rapamycin and ALX-5407 was evaluated through histopathology, immunofluorescence, and splenocyte profiling. Mechanistic insights were derived from RNA-seq, KEGG/GO enrichment, and Western blotting.

Results: GlyT1 expression was significantly upregulated in Th1 cells and rejection cohorts. ALX-5407 suppressed Th1 differentiation, reducing IFN- γ^+ CD4⁺T cells proportions (p < 0.05) and activation markers (CD25, CD69), while inducing apoptosis via caspase-3 activation and BCL-2 downregulation. Although ALX-5407 monotherapy failed to prolong graft survival, combination with rapamycin synergistically enhanced efficacy (p = 0.018), reduced inflammatory infiltration, and attenuated splenic Th1 polarization. Mechanistically, ALX-5407 inhibited MAPK signaling but activated the PI3K-AKT-mTOR pathway, which rapamycin counteracted to amplify suppression.

Conclusions: GlyT1 serves as a metabolic checkpoint in Th1 differentiation, and its inhibition by ALX-5407 attenuates allograft rejection through dual suppression of Th1 function and apoptosis induction. Synergy with rapamycin highlights a novel combinatorial strategy to mitigate rejection with reduced toxicity. These findings position GlyT1 targeting as a promising approach for clinical translation in transplantation immunotherapy.

KEYWORDS

solute carrier, GlyT1, ALX-5407, T-cell-mediated rejection, organ transplantation

1 Introduction

Transplant rejection remains a principal cause of graft loss, driven by dysregulated immune responses in which T helper 1 (Th1) cells play a central role (1, 2). Upon activation, T cells undergo metabolic reprogramming to meet bioenergetic demands, with enhanced glycolysis and mitochondrial oxidative phosphorylation emerging as critical regulatory nodes for effector function (3, 4). This metabolic plasticity not only sustains pro-inflammatory cytokine production but also establishes a potential therapeutic vulnerability. Targeting T cell metabolic pathways, such as glucose utilization or amino acid transport, may offer a promising strategy to attenuate pathological immune activation while preserving homeostatic immunity (5, 6).

Glycine functions as a pleiotropic metabolic hub with significant anti-inflammatory and anti-apoptotic properties (7). It acts as a one-carbon unit donor to drive cellular proliferation and epigenetic reprogramming via the one-carbon cycle, while serving as an essential substrate for glutathione (GSH) biosynthesis to scavenge reactive oxygen species (ROS), thereby alleviating oxidative stress and preserving cellular function. In the context of transplant rejection (8-10), the heightened metabolic activity of CD4+ Th1 cells renders them exquisitely sensitive to alterations in intracellular glycine concentrations (11, 12). Modulation of glycine availability selectively suppresses Th1 cell proliferation and effector functions, consequently attenuating Th1-dominated T cellmediated allograft rejection and ultimately mitigating graft injury to prolong transplant survival. The solute carrier (SLC) transporter family, comprising over 400 membrane proteins, has recently been implicated in T cell metabolic adaptation (13, 14). Specific SLC members, including SLC7A5 (LAT1) and CD98, facilitate the uptake of essential nutrients such as leucine and glutamine, directly fueling mTORC1 signaling and epigenetic modifications during T cell differentiation (15, 16). Dysregulation of SLCmediated metabolic rewiring correlates with aberrant CD4+T polarization in allograft rejection models, positioning this family as a novel immunomodulatory target. Elucidating the interplay between SLC transporters and T cell metabolism could uncover precision mechanisms to mitigate rejection without broadspectrum immunosuppression (17).

SLC6A9(GlyT1), a member of the solute carrier 6 (SLC6) family, encodes the sodium/chloride-dependent glycine transporter 1 (18). GlyT1 transports glycine from the synaptic cleft back into neurons via active transport. ALX-5407, a potent and highly selective glycine transporter-1 inhibitor, effectively reduces glycine influx, leading to extracellular glycine accumulation. In the nervous system, this elevation of synaptic glycine concentration modulates neural plasticity and excitability, offering therapeutic potential for psychiatric disorders. This transporter primarily regulates glycine transmembrane flux and has recently been implicated in modulating mitochondrial glycine metabolism within cells (19). However, its specific mechanistic contributions to transplant rejection remain underexplored, warranting further investigation to elucidate its therapeutic potential in alloimmune regulation. based on the effect of GlyT1 inhibitors on reducing intracellular glycine levels and glycine's critical role in CD4⁺T cell function, we propose the hypothesis that GlyT1 inhibition may modulate CD4⁺T cell activation states. Our study indicates that SLC6A9 plays a role in Th1 differentiation and is a potential target for reducing graft rejection.

2 Materials and methods

2.1 T cell isolation and polarization

Spleens were aseptically harvested from euthanized male C57BL/6 mice (male, 6-8w) and mechanically dissociated into single-cell suspensions. CD4⁺T cells were isolated using magnetic bead-based negative selection kits (STEMCELL) and cultured in anti-CD3ε pre-coated 96-well plates (5μg/mL, BioLegend) under Th1-polarizing conditions: RPMI 1640 medium supplemented with recombinant IL-2 (100 IU/mL, PeproTech), IL-12p70 (10 ng/mL, PeproTech), anti-IL-4 (10μg/mL, BioLegend), and anti-CD28 (2μg/mL, BioLegend). ALX-5407 (MCE HY-10711A) was administered at 0.5–500 nM concentrations, with vehicle-treated cells serving as controls. Cells were harvested after 72-hour stimulation for flow cytometry or RNA sequencing.

2.2 Mouse skin transplantation model

Full-thickness tail skin grafts (1×1 cm) from donor BALB/c mice (male, 6-8w) were transplanted onto the dorsal region of anesthetized C57BL/6 recipients (male, 6-8w) using 6-0 Prolene sutures. Postoperatively, mice received daily intraperitoneal injections of ALX-5407 (100 mg/kg), rapamycin (50 mg/kg), or vehicle (n=5/group). Graft viability was monitored until Day 7, with >90% necrosis defined as rejection. Surviving grafts and secondary lymphoid organs were collected for histopathological and immunological analyses.

2.3 Mouse heart transplantation model

BALB/c mice (male, 6-8w) were anesthetized by inhalation and systemically heparinized via intraperitoneal injection. The thoracic cavity of the mouse was then opened. After the heart stopped beating, the superior vena cava and pulmonary veins of the mouse heart were ligated, and the aorta and pulmonary artery were disconnected. The donor heart was harvested and stored in icecold saline. C57BL/6 mice (male, 6-8w) were anesthetized by inhalation, and the skin on the right neck was incised to locate the right internal jugular vein and the right internal carotid artery. The right internal jugular vein and the right internal carotid artery were ligated, disconnected, and cannulated. The donor heart aorta was then sleeved onto the recipient's internal carotid artery end, and the donor heart pulmonary artery was sleeved onto the recipient's internal jugular vein end. After fixing and ligating the interfaces, blood flow was restored, and the heart filled and restarted beating. After the operation, the recipient mice were anesthetized by inhalation daily, and the beating of the donor heart was assessed

by manual palpation to determine the heart beating situation, and a graft survival curve was plotted.

2.4 Flow cytometry

Single-cell suspensions from *in vitro* cultures or recipient spleens were stained with fluorochrome-conjugated antibodies against surface markers (Live/Dead, CD4, CD8 α , CD25, CD44, CD69, NK1.1, CD19, CD11b, Ly6G, Ly6C, CD11c, F4/80), followed by intracellular fixation/permeabilization for IFN- γ , IL-17A, and Foxp3 detection. For cytokine profiling, cells were stimulated with PMA/ionomycin (1 μ g/mL each, Invitrogen TM) in the presence of brefeldin A (10 μ g/mL, Invitrogen TM) for 6 hours prior to staining. Data acquisition was performed on a BD LSR Fortessa X-20 cytometer and analyzed using FlowJo v10.8.

2.5 qRT-PCR

Total RNA was extracted from The CD4⁺T cells sorted from the spleen and subsequently cultured *in vitro* for 3 days using TRIzol reagent (Invitrogen) and reverse-transcribed into cDNA with PrimeScript RT Master Mix (TransGen). qPCR was performed on a LightCycler[®] 96 system (Roche) using 2X SYBR Green Premix (TransGen) in 10 μ L reactions. Primer pairs were designed via NCBI Primer-BLAST and validated by melting curve analysis. Relative gene expression was calculated using the 2^(- $\Delta\Delta$ Ct) method with GAPDH as endogenous control. All reactions were performed in triplicate.

2.6 H&E staining and immunofluorescence

Transplanted skin grafts and transplanted heart grafts were fixed in 4% paraformaldehyde, paraffin-embedded, and sectioned at 5 µm thickness. Hematoxylin and eosin (H&E) staining was performed using standard protocols (Servicebio) for histopathological evaluation. For CD4 immunofluorescence, antigen retrieval was performed with citrate buffer (pH 6.0, 95°C, 15 min). Sections were blocked with 10% goat serum (Beyotime) and incubated with anti-CD4 primary antibody (1:100, Invitrogen) at 4°C overnight, followed by Alexa Fluor 488-conjugated secondary antibody (1:500, Invitrogen) for 1 h at room temperature. Nuclei were counterstained with DAPI (Servicebio). Images were captured using a Olympus upright fluorescence microscope. Negative controls omitted primary antibodies.

2.7 CFSE proliferation assay and *in vivo* CTV proliferation assay

The CD4 $^+$ T cells sorted from the spleen were labeled with 5 μM CFSE (Invitrogen) in PBS at 37 $^\circ$ C for 10 min, followed by

quenching with complete RPMI-1640 medium. Cells were seeded in 96-well plates and treated with ALX-5407 at concentrations of 0.5, 5, 50, or 500 nM, while control groups received vehicle (0.1% DMSO). After 72 h incubation (37°C, 5% CO₂), cells were harvested and analyzed by flow cytometry (BD LSR Fortessa 20X). Proliferation indices were calculated using FlowJo v10.8 software based on CFSE dilution.

The CD4⁺ T cells sorted from the spleens of C57BL/6 mice were labeled with CellTraceTM Violet (CTV) (20) and activated *in vitro* for 1 day using anti-mouse CD3 (5 ng/ml) and anti-mouse CD28 (2 ng/ml). They were then intravenously infused into C57BL/6 mice, which were randomly divided into an ALX-5407 group and a control group. According to the group, mice received intraperitoneal injections of ALX-5407 (50 mg/kg, once daily)(n=5). Three days later, spleens were collected from the mice for flow cytometry analysis to compare the proliferation of CD4⁺ CTV⁺ cells between the two groups by flow cytometry (BD LSR Fortessa 20X). Proliferation indices were calculated using FlowJo v10.8 software based on CTV dilution.

2.8 RNA sequencing

The CD4⁺T cells sorted from the spleen were polarized into Th0 and Th1 subsets under standard conditions for 3 days. For ALX-5407 treatment, cells were exposed to 500 nM ALX-5407 or vehicle (0.1% DMSO) for 24 h. Total RNA was extracted using TRIzol (Invitrogen), followed by ribosomal RNA depletion and library preparation with NEBNext Ultra II RNA Library Prep Kit (NEB). Differentially Expressed Genes (DEGs) were identified using DESeq2 (|log2FC| >1, adj. p <0.05). Gene Ontology (GO) and KEGG pathway analyses were conducted via clusterProfiler (v4.0).

2.9 Western blotting

The CD4⁺T cells sorted from the spleen and subsequently cultured *in vitro* for 3 days were lysed in RIPA buffer (Beyotime) containing protease inhibitors (Beyotime). Protein concentrations were quantified via BCA assay (Thermo Fisher). Equal amounts (20 µg/lane) were separated by 10% SDS-PAGE gel electrophoresis and transferred onto PVDF membranes (Millipore). After blocking with 5% non-fat milk for 1 h, membranes were incubated overnight at 4° C with primary antibodies as loading control. HRP-conjugated secondary antibodies were applied for 1 h at RT. Signals were detected using ECL chemiluminescence and quantified by ImageJ v1.53.

2.10 Statistical analysis

Data were analyzed using GraphPad Prism v10.0 and expressed as mean ± SD. Multiple group comparisons employed two-way ANOVA with Bonferroni *post hoc* correction. Pairwise comparisons between specific groups used unpaired Student's t-test. Skin

graft survival rates were analyzed by Kaplan-Meier method with log-rank test for significance. p < 0.05 was considered to be statistically significant.

3 Results

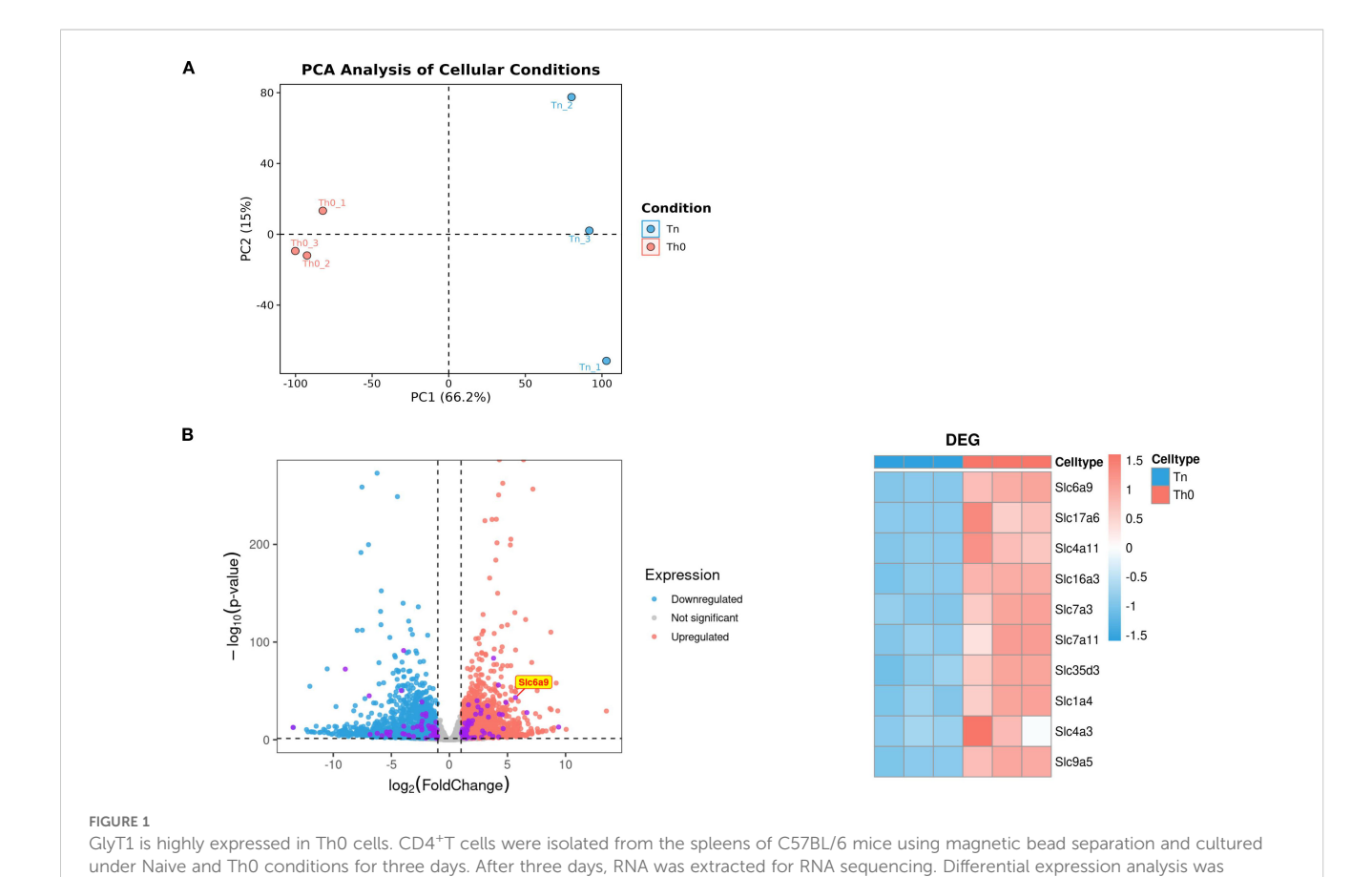
3.1 SLC6A9 (GlyT1) is highly expressed in Th1 cells

To investigate differences between Th0 and Th1 cells, CD4⁺T cells isolated from spleens of male C57BL/6 mice via magnetic bead sorting were cultured under Th0 or Th1 conditions for 3 days. RNA sequencing revealed distinct transcriptomic profiles between Th0 and Th1 cells (Figure 1A). Solute carrier (SLC) family proteins, as primary transporters of intracellular substances, profoundly influence cellular metabolic homeostasis through expression changes. Therefore, we prioritized analysis of differential SLC protein expression between the two experimental groups. Among differentially expressed genes, SLC6A9 (GlyT1), a cell-surface glycine transporter critical for maintaining intracellular/extracellular glycine homeostasis, exhibited significantly higher expression in Th1 cells compared to Th0 cells (p < 0.05, Figure 1B). These findings suggest that GlyT1-mediated glycine regulation may influence Th1 proliferation and differentiation.

(Purple dot) for detailed characterization (B), (n = 3)

3.2 ALX-5407 does not affect the proliferation of CD4⁺ T cells *in vivo* and *in vitro* but impacts the differentiation and function of CD4⁺ Th1 cells

To investigate whether GlyT1 could influence CD4+ T cell proliferation and differentiation, we utilized ALX-5407, a specific inhibitor of GlyT1. According to literature, ALX-5407 selectively inhibits GlyT1 function by reducing glycine transmembrane flux and is currently under experimental investigation for treating neuropsychiatric disorders, with a recommended concentration of 5 nM for neuronal cells. To determine the impact of ALX-5407 on Th1 differentiation and identify effective doses, we treated CFSE-labeled CD4⁺T cells with a concentration gradient (0.5 nM, 5 nM, 50 nM, 500 nM) under Th1-polarizing conditions for 3 days. Flow cytometry results after 3 days showed that ALX-5407 at various concentrations had minimal effects on Th1 cell proliferation (Figure 2A). However, cell viability began to decline at 500 nM, prompting us to select this concentration for subsequent experiments. To further investigate the impact of ALX-5407 on CD4⁺T cells proliferation in vivo, we isolated CD4⁺T cells from the spleens of C57BL/6 mice, labeled them with CTV (20), and activated them in vitro. These cells were then injected into C57BL/6 mice. Flow cytometry analysis of splenocytes 3 days postinjection revealed that the proliferation of CD4⁺CTV⁺cells in the ALX-5407 treatment group appeared moderately reduced compared to the



performed between the two groups (A), with subsequent focus on the top 10 most differentially expressed genes from the solute carrier (SLC) family

control group. However, this result showed no statistical significance, suggesting that, consistent with *in vitro* results, ALX-5407 exerts minimal impact on CD4⁺T cell proliferation *in vivo* (Figure 2B).

However, Flow cytometry analysis revealed that the proportion of CD4⁺IFN- γ ⁺ T cells in the ALX-5407-treated group was significantly lower than in the control group, with IFN- γ MFI also markedly reduced (Figure 2C). Concurrently, MFI values of CD25 and CD69 in the ALX-5407 group decreased, indicating reduced T cell activation (Figure 2D). Further analysis of cytokine mRNA expression levels demonstrated consistent results: *Ifng* expression was significantly downregulated, while $Il1\beta$ and Il10 were upregulated, with no change in Tgfb1 (Figure 2E). These results suggest that ALX-5407, a GlyT1 inhibitor, significantly suppresses Th1 differentiation and impairs Th1 cell activation and function.

3.3 ALX-5407 synergizes with rapamycin to prolong allograft survival

To further validate our findings, we established a BALB/c (male, 6-8 weeks) to C57BL/6 (male, 6-8 weeks) murine skin allograft model. Starting from the day of surgery, four groups received daily intraperitoneal injections: control, ALX-5407 alone, rapamycin alone, and ALX-5407 combined with rapamycin. Graft survival analysis demonstrated that ALX-5407 monotherapy failed to prolong graft survival, while the combination treatment significantly extended survival compared to both single-agent groups (p=0.018, Figure 3A-B). Histological evaluation on day 7 post-transplantation revealed better-preserved graft architecture with reduced inflammatory infiltration in the combination group (Figure 3C). Immunofluorescence analysis further confirmed significantly fewer CD4⁺T cells infiltrating the grafts in the combination group compared to other treatments (Figure 3D and Supplementary Figure 2). These results indicate that ALX-5407 synergizes with rapamycin to exert significantly enhanced protective effects on allografts.

Based on the above skin transplantation results, to further clarify the impact of ALX-5407 on solid organ transplantation, we established a mouse allogeneic heart transplantation model for validation. Experimental data demonstrated that the survival time of the transplanted heart in the ALX-5407 treatment group was significantly prolonged compared with the control group, with a statistically significant difference (Figure 3E, p=0.0020). Pathological analysis of the transplanted heart tissue collected on post-transplantation day 7 revealed that, compared with the control group, the structural integrity of the transplanted heart in the ALX-5407 treatment group was significantly improved, and the degree of inflammatory cell infiltration was notably reduced (Figure 3E).

3.4 ALX-5407 attenuates Th1-driven rejection by modulating splenic immune responses

To investigate the mechanisms underlying the protective effects of ALX-5407 combined with rapamycin on allografts, we performed

flow cytometry analysis on splenocytes from skin-grafted mice at postoperative day 7 (gating strategy shown in Supplementary Figure 1). No significant differences were observed among groups in splenocyte viability, $CD4^+/CD8^+$ T cell ratios, or $CD4^+/CD8^+$ T cell proportions (Figure 4A). Notably, the proportion of $CD4^+IFN-\gamma^+$ T cells was reduced in all treatment groups compared to controls, with the most pronounced reduction in the combination group (Figure 4B). A parallel reduction was observed in $CD8^+IFN-\gamma^+$ T cell frequencies. Furthermore, combination therapy significantly reduced activation marker expression (CD25, CD44, CD69 MFI) in both $CD4^+$ and $CD8^+$ T cells (Figures 4C, D). These findings demonstrate that ALX-5407 and rapamycin synergistically suppress Th1 polarization while attenuating T cell activation.

To determine whether ALX-5407 impacts other T cell subsets, we analyzed regulatory T cells (Tregs) and Th17 cells, which showed no significant intergroup differences (Supplementary Figure 3). Analysis of broader immune populations, including B cells, NK cells, macrophages, dendritic cells, and myeloid-derived suppressor cells, revealed no treatment-associated alterations. Collectively, these data indicate that the anti-rejection efficacy of ALX-5407 combined with rapamycin primarily stems from coordinated inhibition of Th1 differentiation and functional activity.

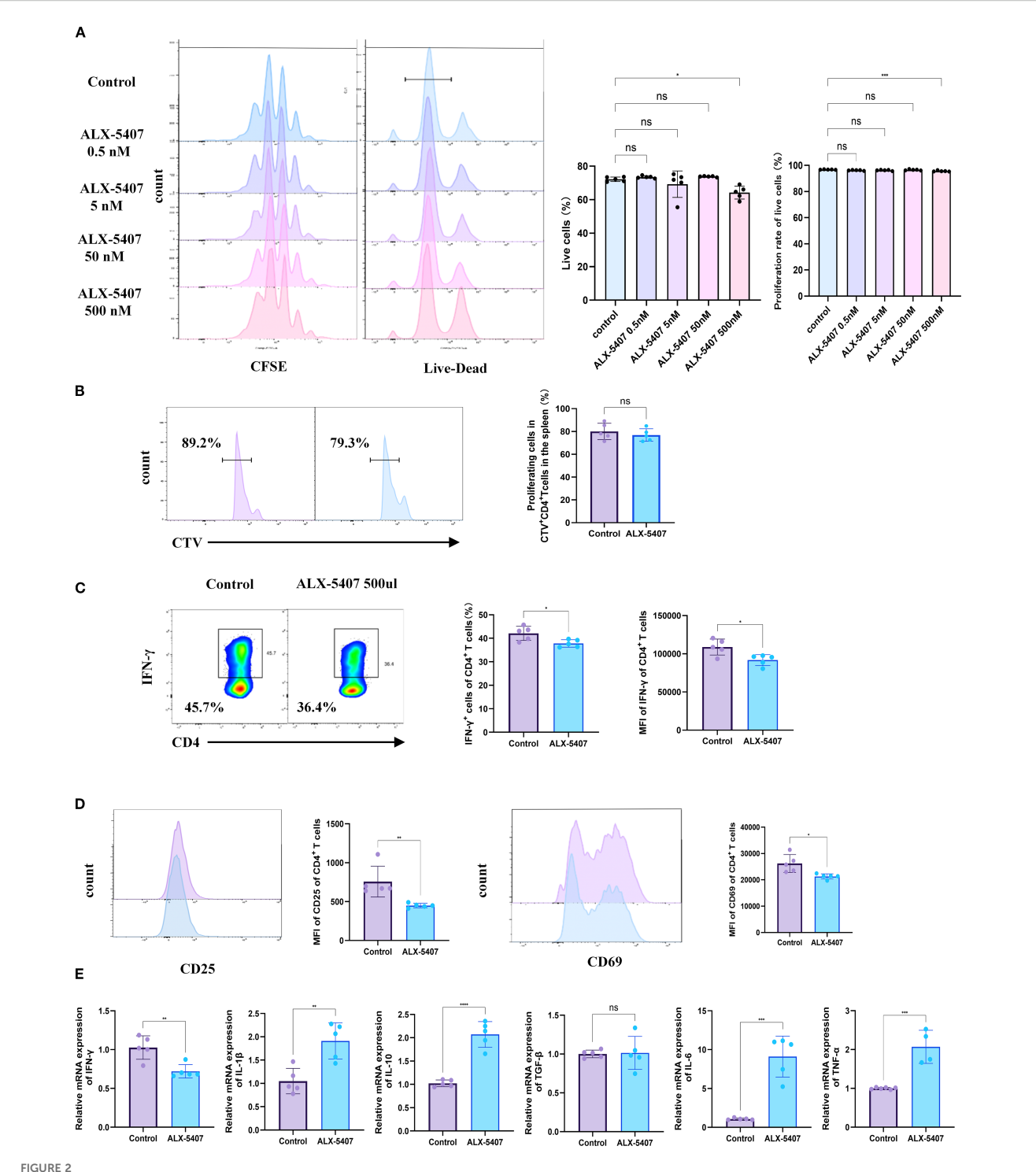
3.5 ALX-5407 suppresses Th1 cell differentiation via apoptosis induction

To investigate the mechanism by which ALX-5407 inhibits Th1 differentiation, we performed RNA sequencing (RNA-seq) on ALX-5407-treated Th1 cells and conducted KEGG/GO enrichment analyses compared to untreated controls (Figures 5A, B). The results revealed significant upregulation of the PI3K-AKT-mTOR pathway and downregulation of the MAPK pathway in ALX-5407-treated cells, which were further validated by Western blot analysis (Figures 5C–E). Given the critical roles of PI3K-AKT-mTOR and MAPK pathways in apoptosis regulation, we assessed apoptotic activity in ALX-5407-treated cells. Apoptosis was significantly increased in the ALX-5407 group (Figure 5F), with Western blot confirming elevated levels of cleaved caspase-3 and reduced expression of the anti-apoptotic protein BCL-2 (Figure 5D) (21, 22). These findings suggest that ALX-5407 reduces the Th1 cell population by inducing cellular apoptosis.

Notably, PI3K-AKT-mTOR pathway activation promotes T cell proliferation and differentiation, potentially explaining the limited efficacy of ALX-5407 monotherapy. Combining ALX-5407 with the mTOR inhibitor rapamycin partially counteracted mTOR pathway activation induced by ALX-5407, resulting in a synergistic enhancement of Th1 suppression (1 + 1 > 2) effect).

4 Discussion

The solute carrier (SLC) superfamily comprises over 65 subfamilies (SLC1-SLC65) and 400+ members with conserved structural features, functioning as transmembrane transporters for ions, metabolites, and



ALX-5407 effectively inhibits Th1 cell differentiation but has limited effects on proliferation. Magnetic bead separation was used to isolate CD4 $^+$ T cells from the spleens of C57BL/6 mice. These cells were then treated with varying concentrations of ALX-5407 (0.5 nM, 5 nM, 50 nM, and 500 nM) in culture medium. The CD4 $^+$ T cells were activated and cultured under Th1 conditions for three days. A portion of the cells were labeled with CFSE and cultured for three days, with the control group serving as a reference. After three days, cells were collected for flow cytometry analysis to assess survival rates (A) and CFSE staining to evaluate proliferation (A). CD4 $^+$ T cells sorted from the spleens of C57BL/6 mice were labeled with Cell Trace Violet (CTV) and activated *in vitro* for 1 day using anti-mouse CD3(5 ng/ml) and anti-mouse CD28 (2 ng/ml). They were then intravenously infused into C57BL/6 mice, which were randomly divided into an ALX-5407 group and a control group. According to the group, mice received intraperitoneal injections of ALX-5407 (50 mg/kg, once daily) (n=5). Three days later, spleens were collected from the mice for flow cytometry analysis to compare the proliferation of CD4 $^+$ CTV $^+$ T cells between the two groups (B). Flow cytometry was also employed to detect the proportion of CD4 $^+$ IFN- γ $^+$ T cells (C) and the mean fluorescence intensity(MFI)of CD25 and CD69 (D). qPCR was performed to examine the mRNA expression of various cytokines in the cells (E). Statistical differences between groups were analyzed using the ANOVA test and T-test. (n =5; *p < 0.05, **p < 0.01, ****p < 0.001, *****p < 0.001, *****p < 0.001 ns:no significance).

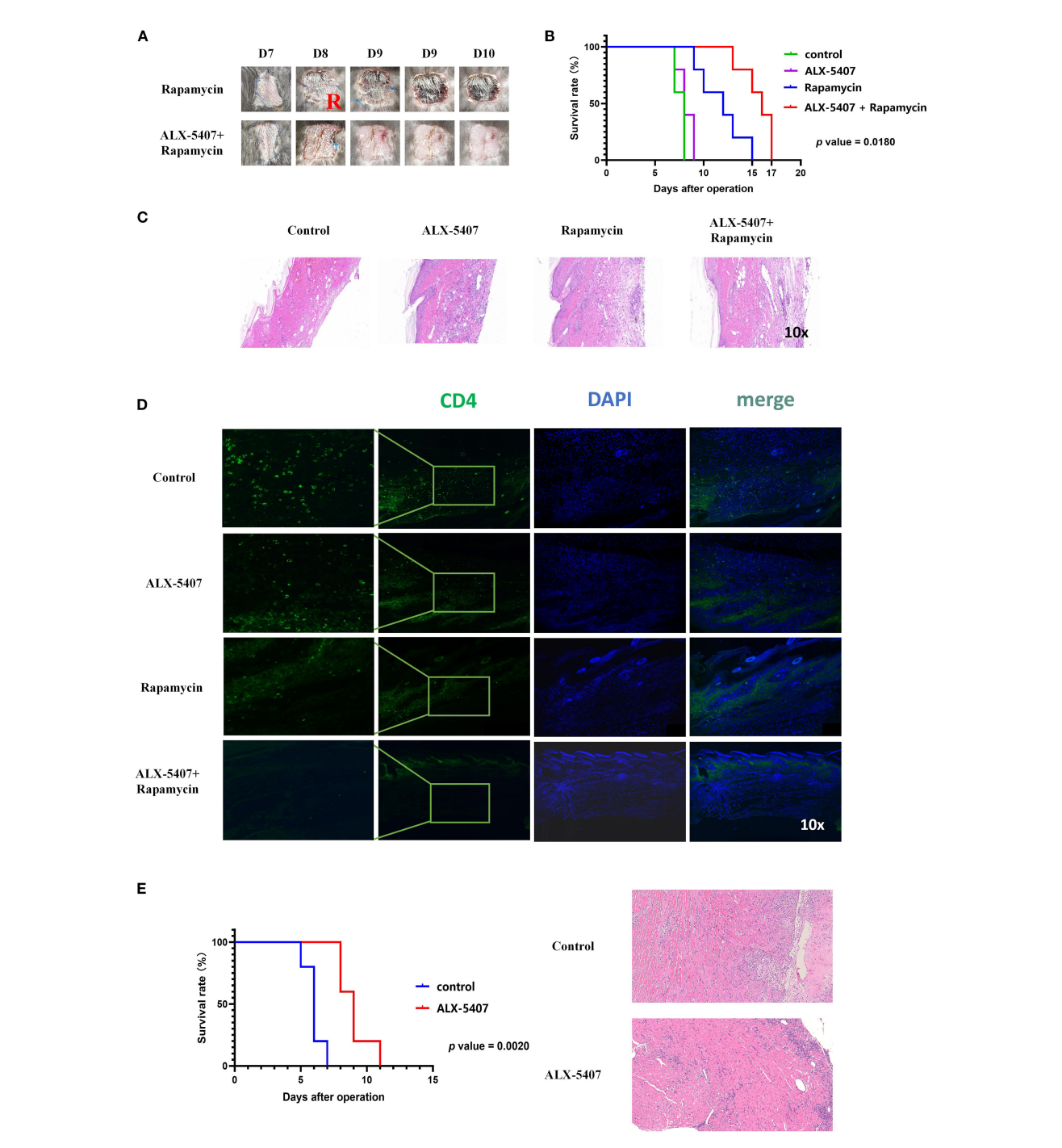
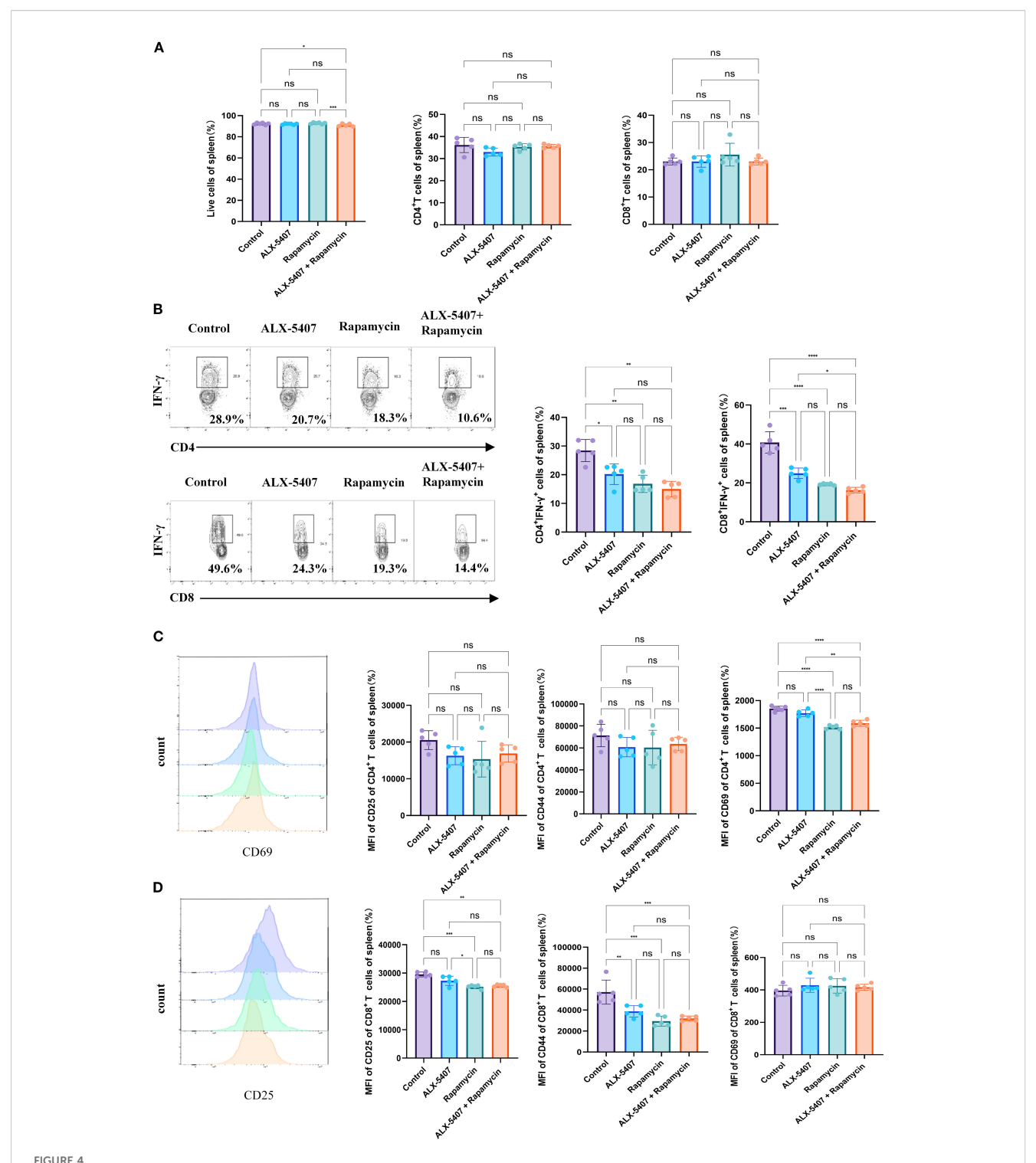


FIGURE 3

ALX-5407 combined with rapamycin effectively prolonged skin allograft survival in mice. BALB/C mouse skin was transplanted onto the backs of C57BL/6 mice, which were randomly divided into two groups: the rapamycin group and the ALX-5407+ rapamycin group. Starting from the day of surgery, the mice in each group were administered daily intraperitoneal injections of rapamycin (50 mg/kg) alone or rapamycin (50 mg/kg) combined with ALX-5407 (100mg/kg). Grafts were photographed daily to assess rejection (A), and survival curves were plotted (B). On postoperative day 7, five mice from each group were randomly selected, euthanized, and their transplanted skin was collected for histological examination using HE staining (C) to evaluate rejection and immunofluorescence staining (D) to assess the infiltration of CD4⁺T cells in the grafts and the mean fluorescence intensity of CD4 expression within each group was analyzed using ImageJ (n=5). Using the cuff technique, cardiac allografts from BALB/c donor mice were heterotopically transplanted into the cervical region of C57BL/6 recipient mice, which were then randomly allocated into four groups: control (no treatment), ALX-5407 (100 mg/kg daily), rapamycin (50 mg/kg daily), and ALX-5407 plus rapamycin (100 mg/kg and 50 mg/kg daily, respectively). Beginning on the day of surgery, mice received daily intraperitoneal injections of the designated treatments, and graft rejection was assessed through daily photographic documentation, and survival curves were plotted (E). On postoperative day 7, five mice from each group were randomly selected, euthanized, and their transplanted heart was collected for histological examination using HE staining (E) to evaluate rejection. Statistical differences between groups were analyzed using the ANOVA test and T-test. (n =5).



ALX-5407 improves graft survival by inhibiting the proportion and function of Th1 cells in skin-transplanted mice. Skin from BALB/C mice was transplanted onto the backs of C57BL/6 mice, which were randomly divided into four groups: a control group, an ALX-5407 group, a Rapamycin group, and an ALX-5407 + Rapamycin group. Daily intraperitoneal injections of the respective drugs were administered post-surgery according to the group assignments. On day 7 after transplantation, the mice were euthanized, and their spleens and peripheral blood were collected for flow cytometry analysis. The proportions of CD4+T cells and CD8+T cells in the spleen (A) and the proportions of CD4+ IFN- γ +T cells and CD8+ IFN- γ +T cells, along with their mean fluorescence intensity (B), were detected. Additionally, the expression levels of CD25, CD44, and CD69 were measured to assess T cell functionality (C, D). Differences between groups were analyzed using ANOVA test. (n =5; *p < 0.05, **p < 0.01, ****p < 0.001, ****p < 0.001 ns:no significance).

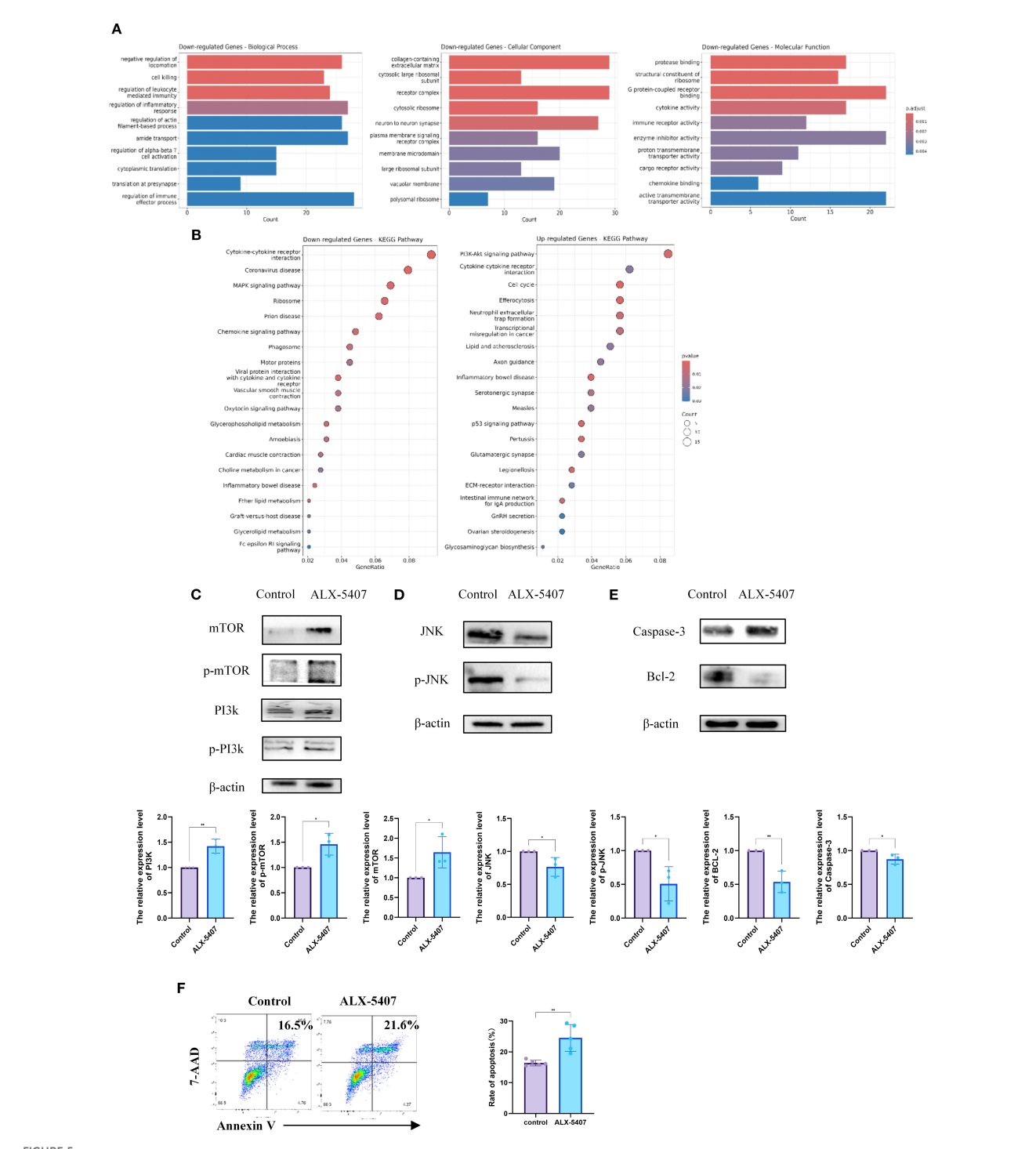


FIGURE 5

ALX-5407 inhibits Th1 cell differentiation by downregulating the MAPK pathway and increasing cell apoptosis. Magnetic bead separation was used to isolate CD4 $^+$ T cells from the spleens of C57BL/6 mice, which were then treated with ALX-5407 (500 nM) in culture medium. The CD4 $^+$ T cells were activated and cultured under Th1 conditions for three days, with the control group serving as a reference. After three days, RNA was extracted from the cells and subjected to RNA-sequencing. Functional analysis was performed using the GO database (A) and KEGG pathway enrichment (B) to identify differentially expressed genes and enriched pathways. Protein was extracted from the cells for Western blot analysis to detect differences in protein expression and the relative expression levels of the protein were compared between the two groups (n=3). (C-E). Additionally, flow cytometry was used to detect differences in cell apoptosis between groups (n=5) (F). Statistical differences between groups were analyzed using the T-test. (*p < 0.05, **p < 0.01 ns:no significance).

pharmaceuticals (23–25). CD4⁺ Th1 cells play a pivotal role in transplant rejection, undergoing metabolic reprogramming with enhanced metabolic activity upon activation and Th1 differentiation (26). SLC family proteins critically participate in these processes and represent promising therapeutic targets for T cell modulation.

GlyT1(SLC6A9), predominantly expressed on neuronal cells, regulates glycine concentrations in neuronal somata and synaptic clefts, and has been explored for neuropsychiatric therapeutics (27–30). Its role in CD4⁺T cell biology remains unclear. Our RNA-seq analysis revealed significant upregulation of GlyT1 during Th0-to-Th1 differentiation, showing the most pronounced expression changes among screened SLC members, thus identifying GlyT1 as our research focus.

Glycine functions as a multifunctional metabolic hub, where its intracellular depletion reduces one-carbon unit availability, thereby limiting S-adenosylmethionine (SAM) biosynthesis (31). This deficiency exerts dual consequences: (1) Diminished provision of C4/C5/N7 atoms essential for purine ring formation impairs thymidylate synthesis, depleting DNA replication substrates and ultimately causing cell cycle arrest with reduced proliferative capacity (32); (2) Compromised methyl donor supply directly disrupts lineage-specific transcriptional programs (attenuated histone modification at the Tbx21 locus), altering epigenetic regulation in CD4⁺T cells (33-35). Concurrently, glycine deficiency inhibits glutathione (GSH) biosynthesis, promoting mitochondrial reactive oxygen species (ROS) accumulation in CD4⁺T cells (36). The inherently low antioxidant capacity in differentiating cells subsequently triggers apoptosis. Experimental GlyT1 inhibition recapitulated this pathophysiology, reducing intracellular glycine and resulting in: elevated caspase-3, suppressed BCL-2, increased CD4⁺T cell apoptosis, and impaired Th1 differentiation. These findings confirm glycine's critical role in CD4⁺ T cell metabolism and demonstrate that targeting its metabolic flux induces functional reprogramming. Notably, in transplantation models, GlyT1 inhibition significantly reduced IFN-γ production in splenic CD8⁺ T cells-a pivotal cytotoxic T lymphocyte (CTL) effector molecule-suggesting parallel mechanisms may attenuate allograft damage, indicative of ALX-5407's broader immunomodulatory potential.

However, unlike previous reports, CD4⁺T cell proliferation remained unaffected. RNA-seq analysis revealed compensatory PI3K-mTOR hyperactivation driving enhanced glycolysis to sustain proliferation. However, this metabolic adaptation simultaneously increased ROS generation and suppressed GSH synthesis, ultimately activating a ROS-BCL-2 axis that establishes the paradoxical "sustained proliferation with accelerated apoptosis" phenotype through failed homeostatic adaptation.

Current conventional immunosuppressive regimens, including glucocorticoids, calcineurin inhibitors (CNIs), mycophenolate mofetil (MMF), and mTOR inhibitors, exhibit notable cytotoxicity and potent immunosuppressive effects that increase risks of malignancies, infections, and systemic toxicities (37–39). This underscores the need for adjuvant immunosuppressive agents with

reduced cytotoxicity that can potentiate conventional therapies while maintaining anti-rejection efficacy. Our findings demonstrate that ALX-5407 monotherapy in murine skin transplantation models showed marginal extension of graft survival compared to controls, though without statistical significance (p>0.05). Given ALX-5407's demonstrated inhibition of Th1 differentiation in vitro, we investigated its combinatorial use with rapamycin. The combined regimen significantly prolonged allograft survival compared to either agent alone (p=0.018), with concomitant suppression of Th1 cell proportions in splenic tissues and CD4⁺ T cell infiltration in grafts. This synergistic effect suggests mutual potentiation between ALX-5407 and rapamycin. Mechanistic analysis revealed that ALX-5407 monotherapy induced paradoxical upregulation of the PI3K-AktmTOR pathway, which is a critical promoter of CD4⁺T cell proliferation/differentiation, potentially explaining its limited standalone efficacy. Crucially, rapamycin coadministration suppressed this feedback activation of mTOR, providing a plausible mechanism for the enhanced anti-rejection effects. This therapeutic strategy establishes a novel paradigm for developing adjuvant immunosuppressants through pathway complementarity (40-42).

Our preliminary evidence suggests ALX-5407 may suppress Th1 differentiation partially through apoptosis induction. Future studies will elucidate its precise molecular targets and optimize its anti-rejection efficacy through mechanism-based engineering.

5 Conclusion

GlyT1 serves as a metabolic checkpoint during Th1 differentiation. Targeting GlyT1 with ALX-5407 reduces Th1 polarization and prolongs allograft survival, likely through apoptosis induction. These findings position ALX-5407 as a novel immunomodulatory agent warranting further development in combination therapies for transplant rejection.

Data availability statement

Bulk RNA-seq data used in the generation of Figures 1 and 5 are available through Gene Expression Omnibus (https://www.ncbi.nlm.nih.gov/geo/) under accession GEO: GSE307193. The original contributions presented in the study are included in the article/Supplementary Material. Further inquiries can be directed to the corresponding authors.

Ethics statement

The animal study was approved by Institute of Radiation Medicine, Chinese Academy of Medical Sciences and Peking Union Medical College. The study was conducted in accordance with the local legislation and institutional requirements.

Author contributions

XZ: Data curation, Conceptualization, Writing – original draft, Formal analysis, Investigation. WZ: Writing – original draft, Funding acquisition, Project administration, Methodology. JW: Project administration, Supervision, Methodology, Investigation, Writing – review & editing. SJ: Writing – review & editing, Investigation, Software, Methodology. ZW: Project administration, Supervision, Methodology, Investigation, Writing – review & editing. HW: Investigation, Supervision, Writing – review & editing, Methodology. GF: Validation, Visualization, Funding acquisition, Supervision, Writing – review & editing. JZ: Resources, Writing – review & editing, Visualization, Supervision, Validation.

Funding

The author(s) declare financial support was received for the research, authorship, and/or publication of this article. This study was supported by Tianjin Natural Science Foundation of Tianjin Science and Technology Bureau (No. 24JCZDJC01380).

Acknowledgments

We would like to express our sincere gratitude to the Experimental Animal Center of the Institute of Radiation Medicine, Chinese Academy of Medical Sciences, for providing the necessary support and approval for the animal experiments conducted in this study. We also thank our colleagues and research staff for their valuable contributions and assistance throughout the research process. We appreciate the guidance and support from all those who contributed to the success of this work. We would like to express our sincere gratitude to Beijing nuohezhiyuan company (service@novogene.com) for the assistance of Bulk RNA-seq in this experiment.

Conflict of interest

The authors declare that the research was conducted in the absence of any commercial or financial relationships that could be construed as a potential conflict of interest.

References

- 1. Louis K, Tabib T, Macedo C, Wang J, Cantalupo P, Chandran U, et al. High-dimensional profiling of immune responses to kidney transplant reveals heterogeneous T helper 1 and B cell effectors associated with rejection. *Am J Transplant.* (2025) 25:706–19. doi: 10.1016/j.ajt.2024.10.009
- 2. Yang Z, Li J, Watanabe H, Gao F, Kawajiri A, Koinuma K, et al. Naturally arising memory-phenotype $\mathrm{CD4}^+$ T lymphocytes give rise to multiple helper subsets to contribute to tumor immunity while inhibiting GVHD. Cancer Immunol Res. (2025). doi: 10.1158/2326-6066.c.7856532
- 3. Ruterbusch M, Pruner KB, Shehata L, Pepper M. *In vivo* CD4(+) T cell differentiation and function: revisiting the th1/th2 paradigm. *Annu Rev Immunol.* (2020) 38:705–25. doi: 10.1146/annurev-immunol-103019-085803

Generative AI statement

The author(s) declare that no Generative AI was used in the creation of this manuscript.

Any alternative text (alt text) provided alongside figures in this article has been generated by Frontiers with the support of artificial intelligence and reasonable efforts have been made to ensure accuracy, including review by the authors wherever possible. If you identify any issues, please contact us.

Publisher's note

All claims expressed in this article are solely those of the authors and do not necessarily represent those of their affiliated organizations, or those of the publisher, the editors and the reviewers. Any product that may be evaluated in this article, or claim that may be made by its manufacturer, is not guaranteed or endorsed by the publisher.

Supplementary material

The Supplementary Material for this article can be found online at: https://www.frontiersin.org/articles/10.3389/fimmu.2025.1644529/full#supplementary-material

SUPPLEMENTARY FIGURE 1

Flow cytometry gating logic diagram showing the detection of cellular proportions *in vitro* and *in vivo* in this study.

SUPPLEMENTARY FIGURE 2

Enlarged images of CD4 immunofluorescence staining in mouse transplanted skin graft sections in Figure 3D, and the comparison of CD4 fluorescence expression levels among different groups.

SUPPLEMENTARY FIGURE 3

ALX-5407 does not statistically significantly affect other cell populations in the spleen of skin-transplanted mice. BALB/C mouse skin was transplanted onto the backs of C57BL/6 mice, which were then randomly divided into four groups: control, ALX-5407, rapamycin, and ALX-5407 + rapamycin. Following the surgery, each group received daily intraperitoneal injections of their respective treatments. Seven days post-surgery, the mice were euthanized, and their spleens and peripheral blood were collected for flow cytometry analysis. The proportions of various cell populations across the groups were compared using ANOVA or T-tests. (n =5;*p < 0.05, ** p < 0.01, *** p < 0.001).

- 4. Fu JY, Huang SJ, Wang BL, Yin JH, Chen CY, Xu JB, et al. Lysine acetyltransferase 6A maintains $\mathrm{CD4^{+}T}$ cell response via epigenetic reprogramming of glucose metabolism in autoimmunity. *Cell Metab.* (2024) 36:557–574 e10. doi: 10.1016/j.cmet.2023.12.016
- 5. Lu Y, Zhao N, Wu Y, Yang S, Wu Q, Dong Q, et al. Inhibition of phosphoglycerate kinase 1 attenuates autoimmune myocarditis by reprogramming CD4+ T cell metabolism. *Cardiovasc Res.* (2023) 119:1377–89. doi: 10.1093/cvr/cvad029
- 6. Sugiura A, Andrejeva G, Voss K, Heintzman DR, Xu X, Madden MZ, et al. MTHFD2 is a metabolic checkpoint controlling effector and regulatory T cell fate and function. *Immunity*. (2022) 55:65–81 e9. doi: 10.1016/j.immuni.2021.10.011

- 7. Zaccherini G, Aguilar F, Caraceni P, Claria J, Lozano JJ, Fenaille F, et al. Assessing the role of amino acids in systemic inflammation and organ failure in patients with ACLF. *J Hepatol.* (2021) 74:1117–31. doi: 10.1016/j.jhep.2020.11.035
- 8. Huang BB, Liu Q, Yu X, Chen YJ, Liang YB, Yu MZ, et al. Integrated analyses to identify the roles of GPX1 in frailty and hypertension. *Hypertension*. (2025) 82:1379–91. doi: 10.1161/HYPERTENSIONAHA.125.24664
- 9. McBride MJ, Hunter CJ, Zhang Z, TeSlaa T, Xu X, Ducker GS, et al. Glycine homeostasis requires reverse SHMT flux. *Cell Metab.* (2024) 36:103–115 e4. doi: 10.1016/j.cmet.2023.12.001
- 10. Lin C, Huang Y, Ran N, Liu J, Luo L, Zhang X, et al. Therapeutic inhibition of HBsAg and HBV cccDNA through a novel phased combination treatment: glycine and interferon-alpha. *Gut.* (2025). doi: 10.1136/gutjnl-2025-334813
- 11. Kabha M, Liaks-Bohnick M, Zagairy F, Atar O, Hamed M, Ziv M, et al. CARMIL2 deficiency disrupts activation-induced metabolic reprogramming in T cells, and is partially rescued by glutamine supplementation. *J Allergy Clin Immunol.* (2025). doi: 10.1016/j.jaci.2025.07.018
- 12. Wang Y, Han Y, Li J, Wang Z, Li K, Bai T, et al. Cell-specific ferroptosis targeting tumors while sparing immune cells. *Biomaterials*. (2025) 323:123457. doi: 10.1016/j.biomaterials.2025.123457
- 13. Cho SY, Kang NS. The solute carrier (SLC) transporter superfamily as therapeutic targets for the treatment of head and neck squamous cell carcinoma. *Cancers (Basel).* (2024) 16. doi: 10.3390/cancers16183226
- 14. Zhou Z, Zhang B, Deng Y, Deng S, Li J, Wei W, et al. FBW7/GSK3beta mediated degradation of IGF2BP2 inhibits IGF2BP2-SLC7A5 positive feedback loop and radioresistance in lung cancer. *J Exp Clin Cancer Res.* (2024) 43:34. doi: 10.1186/s13046-024-02959-3
- Liu H, Deng Z, Yu B, Liu H, Yang Z, Zeng A, et al. Identification of SLC3A2 as a
 potential therapeutic target of osteoarthritis involved in ferroptosis by integrating
 bioinformatics, clinical factors and experiments. *Cells*. (2022) 11. doi: 10.3390/
 cells11213430
- 16. Procaccini C, Garavelli S, Carbone F, Di Silvestre D, La Rocca C, Greco D, et al. Signals of pseudo-starvation unveil the amino acid transporter SLC7A11 as key determinant in the control of Treg cell proliferative potential. *Immunity.* (2021) 54:1543–1560 e6. doi: 10.1016/j.immuni.2021.04.014
- 17. Wei Y, Li R, Meng Y, Hu T, Zhao J, Gao Y, et al. Transport mechanism and pharmacology of the human GlyT1. *Cell.* (2024) 187:1719–1732 e14. doi: 10.1016/j.cell.2024.02.026
- 18. Piniella D, Zafra F. Functional crosstalk of the glycine transporter GlyT1 and NMDA receptors. *Neuropharmacology*. (2023) 232:109514. doi: 10.1016/j.neuropharm.2023.109514
- 19. Li Q, Liu W, Zhang Y, Jin J, Ji P, Yuan Z, et al. ALG5 downregulation inhibits osteogenesis and promotes adipogenesis by regulating the N-glycosylation of SLC6A9 in osteoporosis. *Cell Mol Life Sci.* (2025) 82:35. doi: 10.1007/s00018-024-05566-9
- 20. Zou D, Yin Z, Yi SG, Wang G, Guo Y, Xiao X, et al. $\mathrm{CD4}^+$ T cell immunity is dependent on an intrinsic stem-like program. *Nat Immunol.* (2024) 25:66–76. doi: $10.1038/\mathrm{s}41590-023-01682-\mathrm{z}$
- 21. Wang P, Ma Y, Rao X, Luo Q, Xiao X, Wang T, et al. Kaempferol targets Src to exert its chemopreventive effects on mammary tumorigenesis via regulation of the PI3K/AKT pathway. *Phytomedicine*. (2025) 141:156701. doi: 10.1016/j.phymed.2025.156701
- 22. Jiang H, Lu Q, Huang X, Zhang H, Zeng J, Wang M, et al. Sinomenine-glycyrrhizic acid self-assembly enhanced the anti-inflammatory effect of sinomenine in the treatment of rheumatoid arthritis. *J Control Release*. (2025), 113718. doi: 10.1016/j.jconrel.2025.113718
- 23. Song W, Li D, Tao L, Luo Q, Chen L. Solute carrier transporters: the metabolic gatekeepers of immune cells. *Acta Pharm Sin B.* (2020) 10:61–78. doi: 10.1016/j.apsb.2019.12.006
- 24. Le J, Chen Y, Yang W, Chen L, Ye J. Metabolic basis of solute carrier transporters in treatment of type 2 diabetes mellitus. *Acta Pharm Sin B.* (2024) 14:437–54. doi: 10.1016/j.apsb.2023.09.004

- 25. Newstead S. Future opportunities in solute carrier structural biology. *Nat Struct Mol Biol.* (2024) 31:587–90. doi: 10.1038/s41594-024-01271-0
- 26. Ajmal I, Farooq MA, Duan Y, Yao J, Gao Y, Hui X, et al. Intrinsic ADRB2 inhibition improves CAR-T cell therapy efficacy against prostate cancer. *Mol Ther.* (2024) 32:3539–57. doi: 10.1016/j.ymthe.2024.08.028
- 27. Li N, Wei Y, Li R, Meng Y, Zhao J, Bai Q, et al. Modulation of the human GlyT1 by clinical drugs and cholesterol. *Nat Commun.* (2025) 16:2412. doi: 10.1038/s41467-025-57613-z
- 28. Wang X, Yue M, Cheung JPY, Cheung PWH, Fan Y, Wu M, et al. Impaired glycine neurotransmission causes adolescent idiopathic scoliosis. *J Clin Invest.* (2024) 134. doi: 10.1172/JCI168783
- 29. Le Guellec B, Rousseau F, Bied M, Supplisson S. Flux coupling, not specificity, shapes the transport and phylogeny of SLC6 glycine transporters. *Proc Natl Acad Sci U.S.A.* (2022) 119:e2205874119. doi: 10.1073/pnas.2205874119
- 30. Zhang YW, Uchendu S, Leone V, Bradshaw RT, Sangwa N, Forrest LR, et al. Chloride-dependent conformational changes in the GlyT1 glycine transporter. *Proc Natl Acad Sci U.S.A.* (2021) 118. doi: 10.1073/pnas.2017431118
- 31. Park SH, Ju JS, Woo H, Yun HJ, Lee SB, Kim SH, et al. The m(6)A writer RBM15 drives the growth of triple-negative breast cancer cells through the stimulation of serine and glycine metabolism. *Exp Mol Med.* (2024) 56:1373–87. doi: 10.1038/s12276-024-01235_w
- 32. Johnson AA, Cuellar TL. Glycine and aging: Evidence and mechanisms. *Ageing Res Rev.* (2023) 87:101922. doi: 10.1016/j.arr.2023.101922
- 33. Wu J, Palasantzas V, Andreu-Sanchez S, Plosch T, Leonard S, Li S, et al. Zhernakova, Epigenome-wide association study on the plasma metabolome suggests self-regulation of the glycine and serine pathway through DNA methylation. *Clin Epigenet*. (2024) 16:104. doi: 10.1186/s13148-024-01718-7
- 34. Natoli V, Charras A, Hofmann SR, Northey S, Russ S, Schulze F, et al. DNA methylation patterns in $\mathrm{CD4}^{\scriptscriptstyle +}$ T-cells separate psoriasis patients from healthy controls, and skin psoriasis from psoriatic arthritis. Front Immunol. (2023) 14:1245876. doi: 10.3389/fimmu.2023.1245876
- 35. Teghanemt A, Pulipati P, Misel-Wuchter K, Day K, Yorek MS, Yi R, et al. CD4 expression in effector T cells depends on DNA demethylation over a developmentally established stimulus-responsive element. *Nat Commun.* (2022) 13:1477. doi: 10.1038/s41467-022-28914-4
- 36. Zou Z, Cheng Q, Zhou J, Guo C, Hadjinicolaou AV, Salio M, et al. ATF4-SLC7A11-GSH axis mediates the acquisition of immunosuppressive properties by activated $\mathrm{CD4}^+\mathrm{T}$ cells in low arginine condition. *Cell Rep.* (2024) 43:113995. doi: 10.1016/j.celrep.2024.113995
- 37. Munoz Sandoval D, Bach FA, Ivens A, Harding AC, Smith NL, Mazurczyk M, et al. Plasmodium falciparum infection induces T cell tolerance that is associated with decreased disease severity upon re-infection. *J Exp Med.* (2025) 222. doi: 10.1084/iem.20241667
- 38. Ackermann J, Bernard C, Sirven P, Salmon H, Fraldi M, Ben Amar MD. Mechanistic insight for T-cell exclusion by cancer-associated fibroblasts in human lung cancer. *Elife.* (2025) 13:RP101885. doi: 10.7554/eLife.101885
- 39. Montano-Loza AJ, Rodriguez-Peralvarez ML, Pageaux GP, Sanchez-Fueyo A, Feng S. Liver transplantation immunology: Immunosuppression, rejection, and immunomodulation. *J Hepatol.* (2023) 78:1199–215. doi: 10.1016/j.jhep.2023.01.030
- 40. Koehn BH, Nowak EC, Skopelja-Gardner S, Saha A, Zaiken MC, Allred J, et al. Targeting cell-surface VISTA expression on allospecific naive T cells promotes tolerance. *Blood.* (2025) 145:1687–700. doi: 10.1182/blood.2024025884
- 41. Bachoo S, Gudgeon N, Mann R, Stavrou V, Bishop EL, Kelly A, et al. IL-7 promotes integrated glucose and amino acid sensing during homeostatic CD4 $^{+}$ T cell proliferation. *Cell Rep.* (2025) 44:115199. doi: 10.1016/j.celrep.2024.115199
- 42. Inglis SS, Abbas M, Asleh R, Garmany A, Smith BH, Kushwaha S, et al. Incidence and risk factors for rejection after conversion from calcineurin inhibitor to sirolimus-based immunosuppression in orthotopic heart transplant recipients. *J Heart Lung Transplant*. (2024). doi: 10.1016/j.healun.2024.02.211